

Neutron-Star-Merger Equation of State

Veronica Dexheimer^{1,*}, Constantinos Constantinou¹, Elias R. Most², L. Jens Papenfort²,
Matthias Hanauske^{2,3}, Stefan Schramm^{2,3}, Horst Stoecker^{2,3,4} and Luciano Rezzolla^{2,3}

¹ Department of Physics, Kent State University, Kent, OH 44242, USA; cconsta5@kent.edu

² Institut für Theoretische Physik, Max-von-Laue-Straße 1, 60438 Frankfurt, Germany; most@fias.uni-frankfurt.de (E.R.M.); papenfort@th.physik.uni-frankfurt.de (L.J.P.); hanauske@fias.uni-frankfurt.de (M.H.); schramm@fias.uni-frankfurt.de (S.C.); h.stoecker@gsi.de (H.S.); rezzolla@itp.uni-frankfurt.de (L.R.)

³ Frankfurt Institute for Advanced Studies, Ruth-Moufang-Straße 1, 60438 Frankfurt, Germany

⁴ GSI Helmholtzzentrum für Schwerionenforschung GmbH, 64291 Darmstadt, Germany

* Correspondence: vdexheim@kent.edu

Received: 31 March 2019; Accepted: 22 May 2019; Published: date



Abstract: In this work, we discuss the dense matter equation of state (EOS) for the extreme range of conditions encountered in neutron stars and their mergers. The calculation of the properties of such an EOS involves modeling different degrees of freedom (such as nuclei, nucleons, hyperons, and quarks), taking into account different symmetries, and including finite density and temperature effects in a thermodynamically consistent manner. We begin by addressing subnuclear matter consisting of nucleons and a small admixture of light nuclei in the context of the excluded volume approach. We then turn our attention to supranuclear homogeneous matter as described by the Chiral Mean Field (CMF) formalism. Finally, we present results from realistic neutron-star-merger simulations performed using the CMF model that predict signatures for deconfinement to quark matter in gravitational wave signals.

Keywords: gravitational wave; neutron-star-merger; quark matter

1. Introduction

The first detection of gravitational waves from the neutron-star-merger GW170817 [1], has generated considerable interest in the equation of state (EOS) of matter created in such extreme events. In these events, temperatures of tens of MeV are expected to be generated over regions that vary in density by several orders of magnitude. Therefore, it is imperative to adopt EOS descriptions in which the symmetries and degrees of freedom change according to the local temperature and density conditions of the system. From the point of view of merger simulations, it is important to use a small grid for the simulation to capture the complexity of the event.

In this work, we present a compilation of former works that treated separately the low- and high-density regimes expected to be formed in neutron-star mergers. First, we discuss an extension of the excluded volume (EV) approach, which takes into consideration light nuclei beyond the usual α -particle in the subnuclear regime. Here, the EOS of Akmal, Pandharipande, and Ravenhall (APR) is used as the underlying description for interacting nucleons. Second, for the description of the supranuclear regime, we discuss the Chiral Mean Field (CMF) formalism, in which the hadronic degrees of freedom include both nucleons and hyperons. For sufficiently high temperature and/or density, the CMF model incorporates a first-order phase transition to deconfined quark matter. The merger simulations of this work are performed using a covariant general-relativistic description of hydrodynamics coupled to a fully general-relativistic spacetime evolution. The numerical grid in the simulation achieves the highest resolution of 250 m covering the two stars and a total extent of 1500 km.

2. Subnuclear Density

In this section, we discuss the subnuclear density region, which we take to be $n \lesssim 0.1 \text{ fm}^{-3}$. Besides density, thermodynamic variables also depend on temperature T and electron fraction $Y_e = n_e/n$, the latter being equal to baryonic charge fraction $Y_c = \sum_B Q_i n_i/n$ due to the charge neutrality requirement. In this regime, a uniform phase of nucleonic matter would be mechanically (spinodally) unstable, which would give rise to a negative compressibility. Although this instability shrinks in size with increasing isospin asymmetry (lower electron/charge fraction), it does not disappear for small temperatures. As a solution to the problem, an inhomogeneous phase must be included in the formalism. In our case, it consists (in addition to nucleons and electrons) of light nuclear clusters. As a result, the mechanical instability is lifted for $T \geq 8 \text{ MeV}$. At lower temperatures, mechanically stable configurations must necessarily include heavy nuclei ($A > 4$) and/or pasta phases.

In the EV approach, the α -particles and other light nuclei (${}^3\text{H}$, and ${}^3\text{He}$, and ${}^4\text{He}$) are assumed to be structureless and their interactions with “outside” nucleons are taken into account by treating them as rigid spheres of constant volume. This treatment accounts only for repulsive interactions, the attractive ones being deemed small. The total free energy density can be decomposed as $F = F_b + F_e + F_\gamma$, where the different terms stand for baryon, electron, and photon contributions. The baryon contribution consists of a nuclear contribution given by non-interacting Boltzmann gases and an “outside” nucleon contribution given by the APR EoS.

The APR EOS is a Skyrme-like parametric fit [2] to the microscopic calculations of Akmal and Pandharipande [3], where the NN interaction is described by the Argonne-18 2-body potential, a modified Urbana-IX 3-body potential (so that the binding energy of isospin-symmetric nuclear matter is -16 MeV), and a 2-body relativistic boost potential. The Argonne-18 potential is a high precision fit to the Nijmegen scattering database, such that it reproduces phase shifts and scattering lengths. The Urbana-IX describes 2-pion exchange and includes phenomenological in-medium modifications (involving Δ isobars) to the 2-body interaction. The boost potential is a correction to the 2-body potential when the interaction is observed in a frame other than the rest-frame of the nucleons. The expectation value of the ground state corresponding to the total potential is determined by variational chain summation techniques using a variational wave-function consisting of a symmetrized product of pair-correlation operators acting on the Fermi gas wave-function. As a result, isospin-symmetric nuclear matter equilibrium bulk properties other than n_{sat} and $E/A(n_{sat})$ are predictions of the model, instead of quantities to which it is fitted.

Figure 1, shows a comparison of EV with virial expansion results for $np\alpha$ matter. The virial approach includes bound and continuum state corrections to the ideal gas results for thermal variables [4]. It is model-independent, as experimental phase-shift data are used as input for the theory. The pressure is obtained from the partition function Q according to $P = T/V \log Q$ and it is expressed in terms of the fugacities z_i , ($i = \alpha, n, p$) and the 2nd virial coefficients b_2 , which are simple integrals involving thermal weights and elastic scattering phase shifts. As expected, there are fewer α particles at lower lepton fractions (blue vs. red curves). The APR/EV approach predicts significantly lower α -particle populations at large densities relative to the virial approach (solid vs dashed curves). This is a consequence of only repulsive interactions being included in the EV approach, which is not the case in the virial approach. In the latter, owing to the lack of sufficiently high-energy data such that the nuclear hard-core is resolved, the α -nucleon interaction is predominantly attractive. The sudden disappearance of the α particles causes a change in slope in the baryonic component of thermodynamic quantities. In the case of lower temperatures, this causes a non-monotonic behavior in the baryonic component of thermodynamic quantities. The non-monotonic behavior is smoothed out when other light nuclei are considered (see Ref. [5] for more details).

The mass fractions of the various light nuclear clusters, as calculated by applying the EV approach to the APR EOS, are presented in the left panels of Figures 2 and 3 for temperatures of 5 MeV and 10 MeV, respectively. These are determined by a combination of the charge and baryon number conservation laws, the binding energy of each type of nucleus, and local conditions (n , Y_e , T). The

density at which a particular species vanishes is primarily controlled by the EV v_i assigned to it. In this instance, we are using the corresponding experimentally determined charge radii. Note, however, that this choice is by no means compulsory. For example, in Ref. [6], v_α was obtained by calculating the effective interaction range consistent with an optical potential fitted to neutron- α scattering data. Moreover, the presence of heavy nuclei (not taken into account here) will also affect the relative particle concentrations.

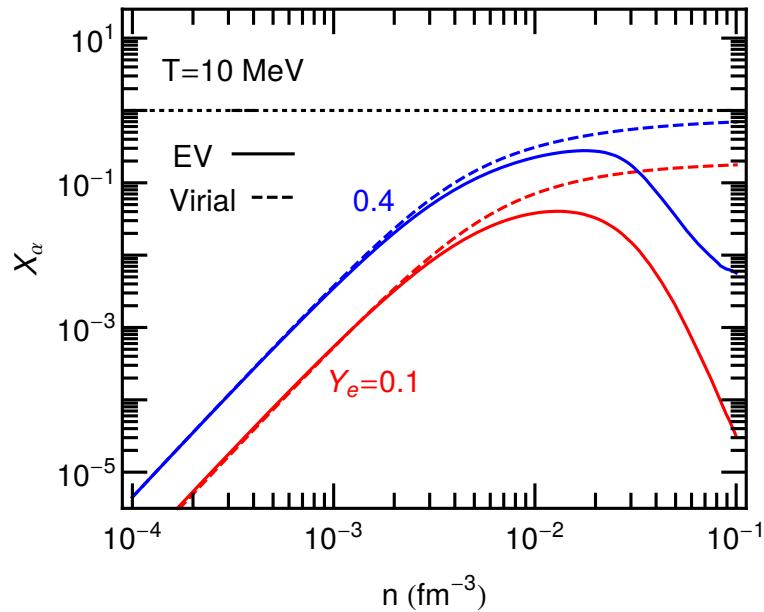


Figure 1. α -particle mass fraction $X_\alpha = 4n_\alpha/n$ as a function of baryon density for different electron fractions at $T = 10$ MeV shown for the APR/excluded volume and virial approaches.

The right panels of Figures 2 and 3 show the contributions of light nuclei, nucleons, and electrons to the total pressure. Being that the light nuclei are treated as non-interacting gases, their pressures are given by classical ideal gas expressions, $P_i = n_i T$, modulated by EV factors. The latter act significantly only at the higher end of the density range considered here and cause the populations of the light nuclei to decline. Please note that electronic contributions dominate at higher densities and even more so as Y_e increases (lower panels). The negative slope in the total pressure around 0.03 fm^{-3} in the bottom right panel of Figure 2 is related to the spinodal instability of purely nucleonic matter (and, therefore, the nuclear liquid-gas phase transition) which is more pronounced at lower temperatures and for more isospin-symmetric configurations. This unphysical behavior is not present in the bottom right panel of Figure 3. Even though the APR liquid-gas critical temperature of about 18 MeV has not been reached in this case, mainly due to electrons, and to a lesser extend to the light nuclei, the total pressure remains monotonically increasing at 10 MeV temperature.

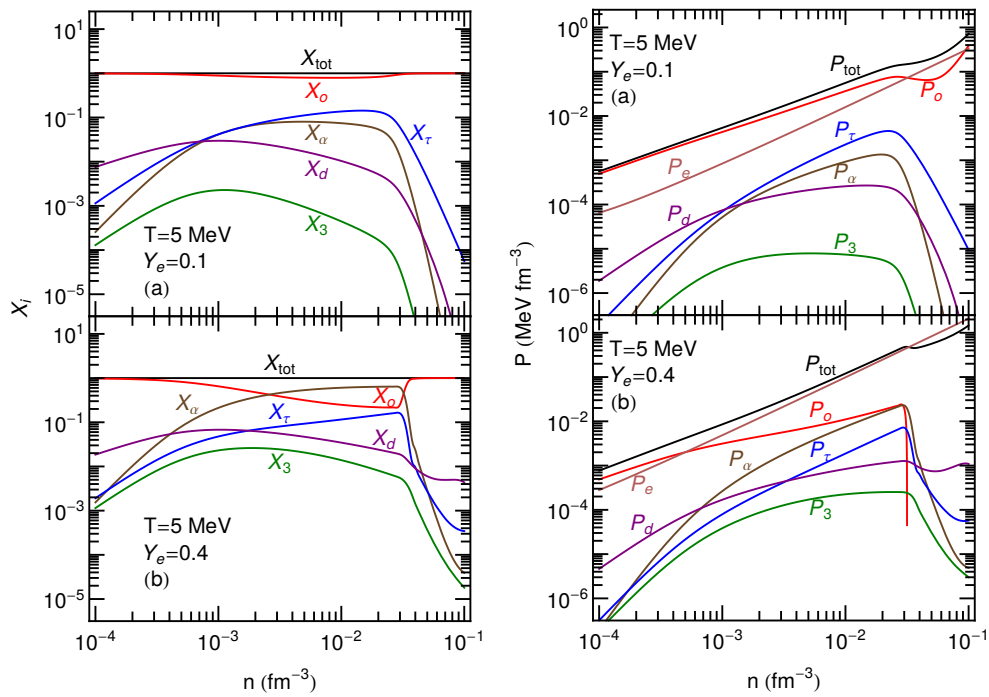


Figure 2. Mass fraction $X_i = A_i n_i / n$ (left) and pressure (right) as a function of baryon density for different electron fractions at $T = 5 \text{ MeV}$ shown for the APR/EV approach. The subscripts $d, \tau, 3, \alpha, e,$ and o correspond to contributions from deuterons, tritons, ^3He , alpha particles, electrons and outside nucleons (nucleons not bound in nuclei). The total mass fraction ($=1$) and total pressure are given by X_{tot} and P_{tot} , respectively.

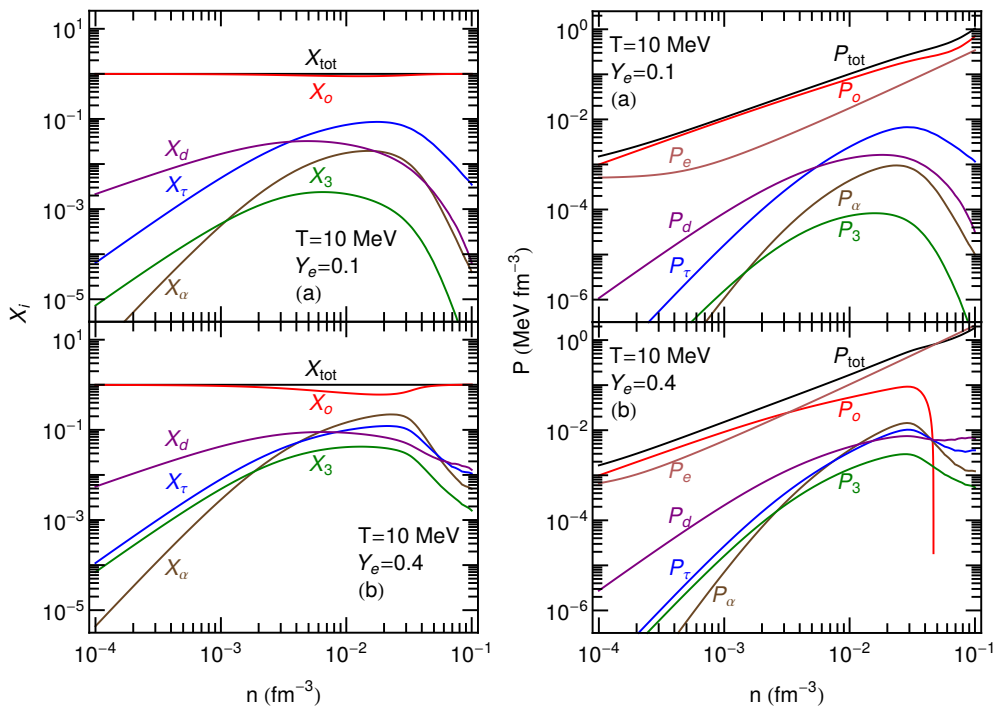


Figure 3. Mass fraction $X_i = A_i n_i / n$ (left) and pressure (right) as a function of baryon density for different electron fractions at $T = 10 \text{ MeV}$ shown for the APR/EV approach. The subscripts $d, \tau, 3, \alpha, e,$ and o correspond to contributions from deuterons, tritons, ^3He , alpha particles, electrons and outside nucleons (nucleons not bound in nuclei). The total mass fraction ($=1$) and total pressure are given by X_{tot} and P_{tot} , respectively.

3. Supranuclear Density

For densities larger than $n \sim 0.1 \text{ fm}^{-3}$, matter is too dense for nuclei of any type to form and, thus, consists of uniformly distributed nucleons and electrons. On one hand, effective field theory has already enabled first-principle calculations of isospin-symmetric and asymmetric matter with systematic corrections. On the other, continuing beyond $n \sim 0.3 \text{ fm}^{-3}$ to encompass the central densities of neutron stars is precluded in these methods, as the perturbative expansion parameter reaches uncomfortably large values (see Ref. [7] for a recent review of the topic). Phenomenological approaches based on non-relativistic potential models with contact and finite-range interactions have long been used to explore the EOS at supranuclear densities, the advantage of these models being that calculations are relatively easier than first-principle calculations. However, higher-than-two-body interactions, found necessary to fit constraints offered by laboratory data on nuclei at near-nuclear densities, can render these EOS's acausal at large density due to the lack of Lorentz invariance in a non-relativistic approach. These higher-than-two-body interactions correspond to terms in the energy density which vary as n^σ with $\sigma > 2$. At sufficiently high densities, they will dominate all other contributions including the thermal parts and lead to superluminal behavior $(c_s/c)^2 \simeq \sigma - 1 > 1$.

As a solution to this problem, relativistic Dirac-Brueckner-Hartree-Fock [8–11] and mean field-theoretical [12] models are used at supranuclear densities, as they and their extensions are inherently Lorentz invariant and, thus, preserve causality. We choose to work with the CMF model, which is based on a nonlinear realization of the SU(3) sigma model [13]. This framework incorporates chiral symmetry and its restoration at large densities and temperatures, as predicted in QCD. Being that hadrons and quarks in the CMF model interact via meson exchange in a chirally invariant manner, the various particle masses originate from interactions with the medium. The model in this specific parametrization is in agreement with standard nuclear and astrophysical constraints [14,15], as well as lattice QCD and perturbative QCD [16,17]. In particular, in the limit of zero-temperature and zero-angular momentum, it predicts a maximum mass of $2.1 M_\odot$ for a hadronic star and $2.0 M_\odot$ when quarks are included.

This approach allows for the existence of soluted quarks in the hadronic phase and soluted hadrons in the quark phase at finite temperature. However, quarks (hadrons) will always give the dominant contribution in the quark (hadron) phase, and the two phases can be distinguished by their approximate order parameters, e.g., the chiral condensate σ for chiral symmetry restoration or the field Φ for deconfinement (named in analogy with the Polyakov loop). This inter-penetration of quarks and hadrons (that increases with temperature) provides a physically effective description and is indeed required to achieve the crossover transition known to take place at small chemical potential values [18]. The left panel of Figure 4 contains the QCD phase diagram (modified from Ref. [19]) resulting from the CMF model and illustrates these features. The right panel in Figure 4 shows the neutron-star matter EOS (assuming charge neutrality and chemical equilibrium) at zero temperature calculated from the CMF model. It can be seen that if the local charge neutrality condition is relaxed to a global charge neutrality condition, a mixed phase appears. In the following, we **are not** going to allow for such relaxation (equivalent to considering a large surface tension between the phases) to study the maximum effect the phase transition can have in binary mergers. We are also going to use a neutrino-leakage scheme to evolve the charge fraction of matter, which will allow us to go beyond the initially chemically equilibrated data.

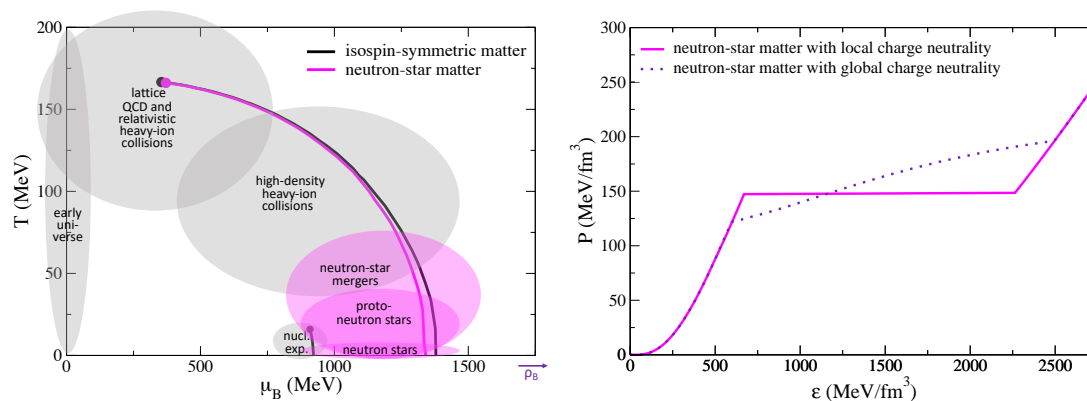


Figure 4. **Left:** QCD Phase diagram resulting from the CMF model. The lines represent first-order transitions. The circles mark the critical end-points. Isospin-symmetric matter refers to zero isospin and strangeness constraints, while neutron-star matter stands for charged neutral matter in chemical equilibrium. The shaded regions exemplify some of the different regimes that can be described within the model. **Right:** EoS for star matter at $T = 0$ under different charge neutrality conditions calculated with the CMF model.

The neutron-star-merger simulations [20] discussed next are performed using the Frankfurt/IllinoisGRMHD code (FIL) [21–24] including weak-interactions via the neutrino-leakage scheme [25–27]. The binaries are initially placed at a distance of 45 km in quasi-circular orbit and perform around five orbits before the merger. These simulations include two setups with equal-mass neutron stars with a combined total mass of $M = 2.8$ and $2.9 M_{\odot}$. For each of these systems, two identical scenarios were simulated either employing the standard CMF EOS, where quarks and a strong first-order PT are included, or a purely hadronic variant, in which the quarks are artificially suppressed.

The left panel of Figure 5 shows the meridional plane for the $2.9 M_{\odot}$ binary 7.7 ms after the merger, when the first-order phase transition has already occurred and formed a hot and dense core inside the hypermassive neutron star. Different subpanels compare simulations performed with the CMF model allowing for quarks (top subpanels) or artificially suppressing quarks (bottom subpanels). The top subpanels show that a large quark fraction is only present in the center and outside ring, where the temperature is high. Please note that in the bottom subpanels, due to the lack of a first-order PT having taken place, there is no hot central region. This feature is a consequence of the sudden compactification generated by the very steep first-order phase transition and would have been significantly less pronounced if a mixture of phases had been included in the EOS.

The right panel of Figure 5 shows which parts of the EOS and the QCD phase diagram are actually probed between 5 ms and 15 ms after the merger for the low-mass binary remnant. The diamonds show the evolution of the maximum baryon density, which basically probes the center of the merged object. The circles show the evolution of the maximum temperature, which probes different regions of the remnant but, eventually, coincides with the center (when circles and diamonds meet). The continued emission of GWs and, hence, the induced loss of angular momentum through GWs leads to a continuous rise of the central density, which ultimately reaches and crosses the boundary of the first-order PT (gray-shaded area).

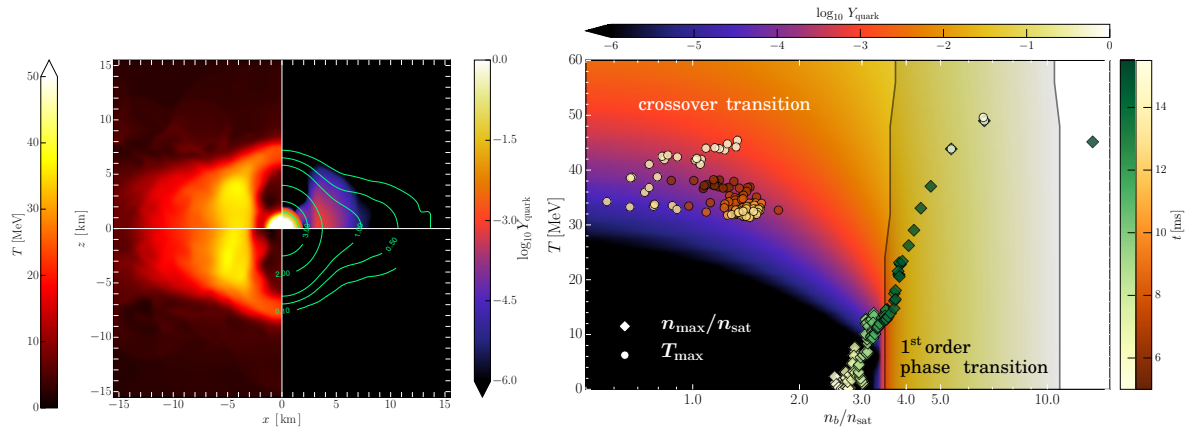


Figure 5. Left: merger simulations performed using the CMF model without (top) and with the suppression of quarks (bottom) for a high-mass binary at a time shortly before the collapse to a black hole (figure extracted from Ref. [20]). Right: time evolution of the maximum normalized baryon density region (diamonds) and maximum temperature region (circles) after the merger for the low-mass binary using the CMF EoS. The gray-shaded area shows the first-order PT being crossed.

In the right panel of Figure 5, the background color code illustrates the relative fraction of quarks compared with the total baryonic one throughout the whole phase diagram. Although it is not shown, the first-order phase transition region will bend left at large temperatures (as indicated in the left panel of Figure 4) but will eventually disappear reaching the crossover region. The first-order phase transition appears in the right panel of Figure 5 as a surface because we show the phase diagram as a function of density and the reason there are points inside the region is (i) due to the way our data was slightly interpolated in that range and (2) the small but finite resolution of the dynamical time-scale of the hydrodynamical simulation. The first-order phase transition would correspond to a line if we had chosen to plot the phase diagram as a function of chemical potential instead. This and other plots will be discussed in a separate publication. Please note that as discussed in detail in Ref. [20], the deconfinement phase transition is enough to produce a dephasing in the gravitational wave form after the merger. This is different from hyperon effects or early quark deconfinement, which should leave imprints in the waveform already before or immediately after the merger [28–30].

4. Discussion and Outlook

Despite advances made in dense nuclear matter theory, many issues remain unresolved and/or poorly constrained with attendant uncertainties in simulations of supernovae and binary mergers of neutron stars. In this work, we explored the effects of light nuclear clusters such as d , ${}^3\text{H}$, ${}^3\text{He}$ and ${}^4\text{He}$ on the properties of the EOS at subnuclear densities. Their interactions among themselves and with nucleons were described in the EV approach. We found that the light cluster relative concentrations are mostly dependent upon the binding energy of the various species. The volume associated with each type of nucleus plays a role only at the higher density range of the subnuclear region and characterizes the population decline of the species at those densities.

We also emphasized that while the EV approach is very useful, it accounts only for repulsive interactions among nuclei and nucleons. We know that attractive interactions are present from phase-shift data and their inclusion in a calculation will certainly provide corrections to the system's state variables. Nevertheless, we expect that these corrections are likely to be small below densities of about 0.01 fm^{-3} , as indicated from a comparison with the virial approach.

Considering supranuclear densities, the CMF model represents a very useful tool to study the influence of different hyperonic and quark degrees of freedom in astrophysical scenarios. This can be seen, for example, in signatures of deconfinement phase transition predicted to exist in neutron-star mergers. Although the differences generated by quarks in this case are not large, they will be possible

to resolve if detected by third-generation GW detectors [31,32], especially in the case that a merger takes place in a nearby system.

While the CMF approach is suitable to describe matter at supranuclear densities (in the neutron-star core), another description is needed for subnuclear densities (the crust and the very low-density regions produced in binary mergers). For the moment, we have matched the CMF EOS to the nuclear statistical equilibrium description presented in Ref. [33], but we are soon going to connect it to the EV approach discussed in this proceeding [5]. This complete table will be made publicly available at CompOSE.

Author Contributions: All authors contributed significantly to this work.

Funding: Support comes from “PHAROS” COST Action CA16214, LOEWE-Program in HIC for FAIR, European Union’s Horizon 2020 Research and Innovation Programme (Grant 671698) (call FETHPC-1-2014, project ExaHyPE), ERC Synergy Grant “BlackHoleCam: Imaging the Event Horizon of Black Holes” (Grant No. 610058), Judah M. Eisenberg - Laureatus Professur at the fachbereich physik at Goethe Universitaet, and the National Science Foundation under grant PHY-1748621. The simulations were performed on the SuperMUC cluster at the LRZ in Garching, on the LOEWE cluster in CSC in Frankfurt, and on the HazelHen cluster at the HLRS in Stuttgart.

Conflicts of Interest: The authors declare no conflict of interest.

References

1. Abbott, B.P.; Abbott, R.; Abbott, T.D.; Acernese, F.; Ackley, K.; Adams, C.; Adams, T.; Addesso, P.; Adhikari, R.X.; Adya, V.B.; et al. GW170817: Observation of Gravitational Waves from a Binary Neutron Star Inspiral. *Phys. Rev. Lett.* **2017**, *119*, 161101.
2. Akmal, A.; Pandharipande, V.R.; Ravenhall, D.G. Equation of state of nucleon matter and neutron star structure. *Phys. Rev. C* **1998**, *58*, 1804.
3. Akmal, A.; Pandharipande, V.R. Spin - isospin structure and pion condensation in nucleon matter. *Phys. Rev. C* **1997**, *56*, 2261–2279.
4. Beth, E.; Uhlenbeck, G.E. The quantum theory of the non-ideal gas. II. Behaviour at low temperatures. *Physica* **1937**, *4*, 915–924.
5. Lalit, S.; Mamun, M.A.A.; Constantinou, C.; Prakash, M. Dense matter equation of state for neutron star mergers. *Eur. Phys. J. A* **2019**, *55*, 10.
6. Lamb, D.Q.; Lattimer, J.M.; Pethick, C.J.; Ravenhall, D.G. Physical properties of hot, dense matter: The general case. *Nucl. Phys. A* **1985**, *432*, 646–742.
7. Tews, I.; Margueron, J.; Reddy, S. Confronting gravitational-wave observations with modern nuclear physics constraints. *arXiv* **2019**, arXiv:1901.09874.
8. M  ther, H.; Prakash, M.; Ainsworth, T.L. The nuclear symmetry energy in relativistic Brueckner-Hartree-Fock calculations. *Phys. Lett.* **1987**, *B199*, 469–474.
9. Engvik, L.; Hjorth-Jensen, M.; Osnes, E.; Bao, G.; Ostgaard, E. Asymmetric Nuclear Matter and Neutron Star Properties. *Astrophys. J.* **1996**, *469*, 794.
10. Baldo, M.; Burgio, G.F. Properties of the nuclear medium. *Rep. Prog. Phys.* **2012**, *75*, 026301.
11. Baldo, M.; Burgio, F., Microscopic Theory of the Nuclear Equation of State and Neutron Star Structure. In *Physics of Neutron Star Interiors*; Blaschke, D., Sedrakian, A., Glendenning, N.K., Eds.; Springer: Berlin/Heidelberg, German, 2001; pp. 1–29.
12. M  ller, H.; Serot, B.D. Relativistic mean-field theory and the high-density nuclear equation of state. *Nucl. Phys. A* **1996**, *606*, 508–537.
13. Papazoglou, P.; Zschesche, D.; Schramm, S.; Schaffner-Bielich, J.; Stoecker, H.; Greiner, W. Nuclei in a chiral SU(3) model. *Phys. Rev. C* **1999**, *59*, 411–427.
14. Dexheimer, V.; Schramm, S. Proto-Neutron and Neutron Stars in a Chiral SU(3) Model. *Astrophys. J.* **2008**, *683*, 943–948.
15. Negreiros, R.; Dexheimer, V.A.; Schramm, S. Modeling Hybrid Stars with an SU(3) non-linear sigma model. *Phys. Rev. C* **2010**, *82*, 035803.
16. Dexheimer, V.A.; Schramm, S. A Novel Approach to Model Hybrid Stars. *Phys. Rev. C* **2010**, *81*, 045201.
17. Roark, J.; Dexheimer, V. The Deconfinement Phase Transition in Proto-Neutron-Star Matter. *Phys. Rev. C* **2018**, *26*, 055805.

18. Aoki, Y.; Endrodi, G.; Fodor, Z.; Katz, S.D.; Szabo, K.K. The Order of the quantum chromodynamics transition predicted by the standard model of particle physics. *Nature* **2006**, *443*, 675–678.
19. Dexheimer, V.; Hempel, M.; Iosilevskiy, I.; Schramm, S. Phase transitions in dense matter. *Nucl. Phys. A* **2017**, *967*, 780–783.
20. Most, E.R.; Papenfort, L.J.; Dexheimer, V.; Hanauske, M.; Schramm, S.; Stocker, H.; Rezzolla, L. Signatures of quark-hadron phase transitions in general-relativistic neutron-star mergers. *Phys. Rev. Lett.* **2019**, *122*, 061101.
21. Del Zanna, L.; Zanotti, O.; Bucciantini, N.; Londrillo, P. ECHO: A Eulerian conservative high-order scheme for general relativistic magnetohydrodynamics and magnetodynamics. *Astron. Astrophys.* **2007**, *473*, 11–30.
22. Borges, R.; Carmona, M.; Costa, B.; Don, W. An improved weighted essentially non-oscillatory scheme for hyperbolic conservation laws. *J. Comput. Phys.* **2008**, *227*, 3191–3211.
23. Harten, A.; Lax, P.D.; van Leer, B. On Upstream Differencing and Godunov-Type Schemes for Hyperbolic Conservation Laws. *SIAM Rev.* **1983**, *25*, 35.
24. Galeazzi, F.; Kastaun, W.; Rezzolla, L.; Font, J.A. Implementation of a simplified approach to radiative transfer in general relativity. *Phys. Rev. D* **2013**, *88*, 064009.
25. Ruffert, M.; Janka, H.T.; Schaefer, G. Coalescing neutron stars—A step towards physical models. I. Hydrodynamic evolution and gravitational-wave emission. *Astron. Astrophys.* **1996**, *311*, 532–566.
26. Rosswog, S.; Liebendörfer, M. High-resolution calculations of merging neutron stars-II. Neutrino emission. *Mon. Not. R. Astron. Soc.* **2003**, *342*, 673–689.
27. O’Connor, E.; Ott, C.D. A new open-source code for spherically symmetric stellar collapse to neutron stars and black holes. *Class. Quantum Grav.* **2010**, *27*, 114103.
28. Sekiguchi, Y.; Kiuchi, K.; Kyutoku, K.; Shibata, M. Effects of Hyperons in Binary Neutron Star Mergers. *Phys. Rev. Lett.* **2011**, *107*, 211101.
29. Radice, D.; Bernuzzi, S.; Del Pozzo, W.; Roberts, L.F.; Ott, C.D. Probing Extreme-density Matter with Gravitational-wave Observations of Binary Neutron Star Merger Remnants. *Astrophys. J. Lett.* **2017**, *842*, L10.
30. Bauswein, A.; Bastian, N.U.F.; Blaschke, D.B.; Chatziioannou, K.; Clark, J.A.; Fischer, T.; Oertel, M. Identifying a first-order phase transition in neutron star mergers through gravitational waves. *Phys. Rev. Lett.* **2019**, *122*, 061102.
31. Punturo, M.; Abernathy, M.; Acernese, F.; Allen, B.; Andersson, N.; Arun, K.; Barone, F.; Barr, B.; Barsuglia, M.; Beker, M.; et al. The third generation of gravitational wave observatories and their science reach. *Class. Quant. Grav.* **2010**, *27*, 084007.
32. Abbott, B.P.; Abbott, R.; Abbott, T.D.; Abernathy, M.R.; Ackley, K.; Adams, C.; Addesso, P.; Adhikari, R.X.; Adya, V.B.; Affeldt, C.; et al. Exploring the Sensitivity of Next Generation Gravitational Wave Detectors. *Class. Quant. Grav.* **2017**, *34*, 044001.
33. Da Silva Schneider, A.; Roberts, L.F.; Ott, C.D. A New Open-Source Nuclear Equation of State Framework based on the Liquid-Drop Model with Skyrme Interaction. *arXiv* **2017**, arXiv:1707.01527v2.

